Theoretical Modeling of Laser Ablation of Quaternary Bronze Alloys: Case Studies Comparing Femtosecond and Nanosecond LIBS Experimental Data

7 AUTHORS, INCLUDING:

A. Santagata
Italian National Research Council
99 PUBLICATIONS   **1,046** CITATIONS

SEE PROFILE

Roberto Teghil
Università degli Studi della Basilicata
161 PUBLICATIONS   **1,771** CITATIONS

SEE PROFILE

Asmaa Elhassan
Higher Technological Institute
10 PUBLICATIONS   **121** CITATIONS

SEE PROFILE

Harith
Cairo University
95 PUBLICATIONS   **931** CITATIONS

SEE PROFILE

Theoretical Modeling of Laser Ablation of Quaternary Bronze Alloys: Case Studies Comparing Femtosecond and Nanosecond LIBS Experimental Data[†]

Lucilla Fornarini,[‡] Roberta Fantoni,*[,‡] Francesco Colao,[‡] Antonio Santagata,[§] Roberto Teghil,[⊥] Asmaa Elhassan,[#] and Mohamed A. Harith[#]

ENEA, FIM-FISLAS, Via E. Fermi 45, I-00044, Frascati (RM), Italy, CNR-IMIP Unità Operativa di Potenza, Zona Industriale, 85050 Tito Scalo (PZ), Italy, Dip. Chimica, Università degli Studi della Basilicata, Via N. Sauro 85, 85100 Potenza, Italy, and National Institute of Laser Enhanced Science, Cairo University, Giza, Egypt

A model, formerly proposed and utilized to understand the formation of laser induced breakdown spectroscopy (LIBS) plasma upon irradiation with nanosecond laser pulses at different fluences and wavelengths, has been extended to the irradiation with femtosecond laser pulses in order to control the fractionation mechanisms which heavily affect the application of laser-ablation-based microanalytical techniques. The model takes into account the different chemico-physical processes occurring during the interaction of an ultrashort laser pulse with a metallic surface. In particular, a two-temperature description, relevant to the electrons and lattice of the substrate, respectively, has been introduced and applied to different ternary and quaternary copper-based alloys subjected to fs and ns ablation both in the visible (527 nm) and in the UV (248 nm). The model has been found able to reproduce the shorter plasma duration experimentally found upon fs laser ablation. Kinetic decay times of several copper (major element) emission lines have been examined together with those relevant to the main plasma parameters. The plasma experimental temperature, derived assuming a Boltzmann distribution, and the electron density following the Saha equation have been compared with the corresponding theoretical data. A satisfactory description of plasma parameters and main matrix constituent composition has been obtained in the time window where local thermal equilibrium was assumed for LIBS data analysis. Improved analytical capabilities are predicted upon delayed detection of plasma emission in femtosecond LIBS, in relation to the better LOD achieved and to the improved data reproducibility expected. Results support the utilization of ultrafast laser sources for trace detection, despite the residual fractionation occurring in the examined range of fluences which affects the linearity of experimental calibration curves built for tin and lead after internal standardization on copper. The validation of model results by experimental data allowed highlighting, from first principles, of the ablation mechanisms for the two temporal regimes and information on how this affects the accurate microanalysis of Cu-based alloys.

1. Introduction

It is well-known that laser ablation (LA) can be employed as a microsampling tool in several analytical techniques requiring prompt vaporization/atomization and the possibility of synchronization with a chosen detection system suitable to time-resolved operation.[1] The two most common examples of successful applications, leading to quantitative analytical analysis, are laser ablation-inductively coupled plasma (LA-ICP)[2] and laser-induced breakdown spectroscopy (LIBS).[3] Both techniques rely on the assumption of the absence of fractionation[4] during the fast vaporization, with an atomization phase passing through plasma formation.[5] Despite considerable expectations, the achievement of a methodology suitable to quantitative trace detection for all elements embedded in different matrixes has not been reached yet in either case; remarkable examples of open questions still are glasses[6] and some copper-based alloys where even main constituents are difficult to accurately determine.[7,8] The fractionation of elements, originally introduced

by Fryer[4] for LA-ICP, is relevant to processes occurring during both laser sampling and the successive vapor transport, and therefore, it is defined on a rather long time scale (minutes, in which trains of laser pulses interact with the sample surface). A different definition of fractionation applies to LIBS, where laser sampling and contemporary plasma formation at high irradiation fluences should be considered for a single laser pulse (up to a few tens of microseconds) and where it is intended as the difference in plasma stoichiometry with respect to the sample surface.[9]

Significant research efforts have been devoted to reduce fractionation in LIBS analysis by employing different laser parameters, and its dependence on laser beam properties has been evaluated.[10,11] The utilization of ultrashort pulses in the femtosecond (fs) range, the wavelength displacement toward the UV range, and the larger and larger energy impinging on the target had some beneficial effects in reducing fractionation. However, final indications for quantitative analyses based on a mere phenomenological description of the effect of laser parameter variations, such as wavelength, fluence, and pulse duration, have not been obtained yet.

In order to understand the vaporization mechanism, which heavily affects the development of LA-based microanalytical techniques, different simplified models were previously devel-

Modeling of Laser Ablation of Quaternary Bronze Alloys

J. Phys. Chem. A, Vol. 113, No. 52, 2009 **14365**

oped to account for the behavior of pure metals in vacuum and in controlled atmosphere. Former work, taking into account the hydrodynamics during the plume physical expansion, was either aimed to support LA-ICP and LIBS[12] or LA-AES and LIBS;[13] in the latter, special attention has been dedicated to plasma space inhomogeneity during the expansion more than to time evolution. The kinetics of reactions was neglected in both cases and carefully considered only in models limited to mere plasma evolution.[14]

A model suitable to investigate the process in copper-based alloys has been formerly proposed and utilized to understand the formation of the LIBS plasma upon irradiation with nanosecond (ns) pulses at different fluences and wavelengths.[15,16] In these works, the effect of both parameters has been clarified, although a satisfactory stoichiometric vaporization has never been achieved (neither theoretically nor experimentally) for both bronze and brass alloys in the investigated experimental conditions.[15,16]

Quantitative LIBS analysis of ancient copper alloys resulted indeed in a complex task,[17] as significant differences in composition between the ablated plasma and the solid sample were generally found, mostly due to differences in physical properties of the metal constituents of these alloys (Cu, Sn, Zn, Pb). Experiments comparing the analysis of copper-based alloys by fs and ns laser pulses[18] up to now did not clearly demonstrate the advantage of using a specific pulse duration at different laser fluences and wavelengths.

In the present work, the model has been extended to take into account the different chemico-physical processes relevant to the interaction of an ultrashort laser pulse with a metallic surface and the generated plasma. In particular, a two-temperature description, relevant respectively to the electrons and lattice of the substrate, is introduced and applied to different ternary and quaternary copper-based alloys subjected to fs ablation in the visible (527 nm) and in the UV (248 nm) ranges. Kinetic decays of different lines for the major element (Cu) are examined in detail, and model predictions are compared to experimental results obtained with different setups operated in similar geometrical arrangements at selected laser fluences, both utilizing fs and ns laser pulses.

Concerning plasma dynamics, although nonequilibrium phenomena have been observed and discussed in LIBS analysis of metal targets,[19,20] quantitative data reduction is usually performed assuming the occurrence of a local thermal equilibrium (LTE) during the entire time window utilized for optical data acquisition; such a slowly varying condition can indeed be established in plasma after a sufficiently long delay from the laser onset and for a definite time window. Whenever LTE conditions occur, electrons, atoms, and ions in plasma can be associated with the same average temperature (with the corresponding Boltzmann distribution of energy levels) and electron density (which, in turn, rules out the ratio of atomic to ionic species through the Saha equation).[21] A partial LTE (pLTE) can also be defined for LTE conditions limited to atoms and ions.[22] In the present work, the time evolution of plasma parameters and atomic emission lines from the main matrix constituent (Cu) have been investigated, and relevant time decay have been obtained both theoretically and experimentally in order to validate the LA models developed.

Usually in LIBS analysis, different elemental concentrations are retrieved either using calibration curves[23] measured on standards with a similar matrix composition or adopting a calibration-free procedure,[24] which requires the detection of all elements present in the unknown sample. In the present work,

theoretical and experimental calibration curves are obtained, based on an internal standardization method, which allow determination of the concentration of constituents different from copper (i.e., Sn, Zn, and Pb), provided that copper is the main matrix element.

The model has also been utilized to predict the time evolution of the signal emitted at a specific element wavelength with respect to the spectrally flat plasma continuum (background) in order to check the behavior of the signal-to-background ratio at delayed plasma emission detection in fs-excited LIBS, which might support the utilization of ultrashort sources for minor elements and trace detection. Among the analytical figures of merit, accuracy in concentration measurements has been considered, as well from the model point of view.

In short, the aim of the present work is to highlight, from first principles, the ablation mechanisms at two temporal regimes and how the process affects the quantitative microanalysis of Cu-based artifacts.

2. Theory and Models

In this section, theoretical considerations relevant to the description of the laser ablation process followed by plasma formation and decay, peculiar to LIBS experiments, are reported and discussed. The section is articulated in two parts; in the first one, the LA model adopted for ns pulse interaction with the alloy surface is presented, and details of the approach relevant to fs pulses interaction are given at the end of it; in the second part, current LIBS data analysis procedures, relying on the LTE assumption, are shortly recalled in order to support the comparison between data retrieved for significant experimental parameters and relevant model predictions, thus validating the latter.

2.1. LA Models. A theoretical model, previously developed for laser ablation of quaternary Cu alloys and described in detail elsewhere,[15] is applied in this work to plasma irradiation of reference ternary and quaternary copper-based alloys (usually named bronzes or brasses, according to the major presence of copper and tin or copper and zinc, respectively). The model, fully developed for simulating the ablation process with ns pulse duration, has already proven to be able to properly reproduce the effects of laser fluence and wavelength variations, the latter from IR (1064 nm) to near-UV (355 nm).[16] In the following, we resume the main features of the modeling assumptions for ns laser irradiation and present the upgraded model introduced to simulate fs irradiation. In both cases, the model will be applied to simulate experimental ablation performed at two different laser wavelengths in the visible (near 530 nm) and in the UV (at 248 nm). The output of the simulation also includes the element concentrations in the laser-produced plasma, starting from known sample composition, to determine plasma stoichiometry and permits a straightforward comparison with experimental calibration curves. By means of these kinds of models, it is possible to follow the evolution of plasma parameters (temperature and electron density), as well as to perform kinetic studies on single lines of different plasma constituents.

2.1.1. Modeling LA with ns Pulses. During the interaction of a ns laser with a solid target, the absorbed laser energy, if sufficiently high, heats the surface first to the melting point and then to the vaporization temperature. If the laser beam size is much larger than the absorption length, it is homogeneous in energy and the lateral heat diffusion is neglected; the heating process can be described by the following one-dimensional heat diffusion equation

$$\rho c_{\rm p}(T)\frac{\partial T}{\partial t} = \frac{\partial}{\partial x}\left(K(T)\frac{\partial T}{\partial x}\right) + S(x,t) \quad (1)$$

where $K(T)$ is the thermal conductivity, T is the temperature, ρ is the density, and $c_{\rm p}(T)$ is the specific heat capacity. $S(x,t) = (1 - R(T))W(t)e^{-\alpha(T)x}$ is the heat generation function at position x and time t, which depends on the optical absorption coefficient α, the surface reflectivity R, and the time evolution of the laser beam power $W(t)$. A Gaussian temporal beam profile was usually considered in the simulations.

The vapor is assumed to leave the target at the surface temperature $T_{\rm s}$ with ionized and neutral species in their equilibrium proportion according to the Saha equation. The populations of the excited levels have been estimated from the population of the ground-state N_0 by using the known Boltzmann relation. Plasma is considered homogeneous in temperature and uniform in density.

Plasma temperature and plume stoichiometry dependence on the material properties are derived from thermal vaporization as this is the main mechanism involved in ns LA under typical experimental conditions.[17,25] Multiphoton ionization and coulomb ejection have been neglected since, in the case of metal surfaces, their contribution is small in the considered time scale of laser pulse duration. In fact, as reported in Stoian, R. et al.,[26] in semiconductors and metals, the high electron mobility and density of available free electrons ensure effective screening and a small net positive charge accumulation during the laser pulse, which is not sufficient, by orders of magnitude to induce a macroscopic electrostatic breakup of the outer layers of the substrate.

The molar flux of evaporating atoms has been calculated by the Hertz−Knudsen equation[27]

$$\frac{d\mu}{dt} = 0.82\frac{P_{\rm sat}}{(2\pi m_{\rm w}R_{\rm G}T_{\rm lv})^{1/2}} \quad (2a)$$

where $m_{\rm w}$ is the molecular weight, 0.82 is a coefficient accounting for the back flow of the evaporated vapor to the surface, $P_{\rm sat}$ is the equilibrium vapor pressure, $T_{\rm lv}$ is the interfacial evaporation temperature corresponding to $P_{\rm sat}$, and $R_{\rm G}$ is the gas constant.

The mass flux per unit surface of evaporating atoms can be expressed as the sum of the following contributions

$$\frac{d\mu}{dt} = \frac{d\mu_0}{dt} + \sum_{n=1}^{M}\frac{d\mu_n}{dt} + \frac{d\mu_{\rm i}}{dt} + \frac{d\mu_{\rm e}}{dt} \quad (2b)$$

with

$$\frac{d\mu_{\rm e}}{dt} = \frac{m_{\rm e}}{M}\frac{d\mu_{\rm i}}{dt} \quad (2c)$$

where μ_0 refers to the ground-state neutrals, μ_n the excited-state neutrals, $\mu_{\rm e}$ the electrons, and $\mu_{\rm i}$ the ions; $m_{\rm e}$ and M are the electron and atom masses, respectively.

We accurately examined the magnitude of the possible processes going on in the plasma which contribute to its temperature and electron density. For the experimental conditions reported, the following have been considered sufficiently important, as already discussed in the paper by Fornarini et al.[15] In particular, two dominant laser absorption mechanisms in the vapor have been considered, inverse Bremsstrahlung and photoionization, whereas the following particle collision processes have been taken into account, electron impact (EI) excitation/de-excitation of neutral atoms, electron impact ionization, and electron capture by an atom through a three-body recombination.[28] Reaction rates for plasma absorption, excitation/de-excitation, and three-body recombination have been calculated as already described in the paper Fornarini et al.[15]

The effective degree of ionization of the laser-produced plasma results from the balance between all of the ionization and recombination mechanisms. These, in turn, depend on the plasma temperature, which is governed by the transfer of electron energy to massive particles by collisions, as heat is being drained from electrons into the coolest heavy particles by elastic collisions.[28]

Taking into account all of these processes, we have been able to derive the species' concentrations and electron and heavy particle temperature in the plasma.[28] These contributions lead to the following system of rate equations for electron ($N_{\rm e}$) and ion number densities ($N_{\rm i} \sim N_{\rm e}$), excited- (N_n) and ground-state neutrals (N_0), and electron ($T_{\rm e}$) and massive particle ($T_{\rm p}$) temperatures.

$$\frac{dN_{\rm e}}{dt} = \frac{dN_{\rm i}}{dt} = \frac{d\mu_{\rm e}}{dt}\frac{1}{z_{\rm p}m_{\rm e}} + \sum_{n=0}^{M}(\alpha_n N_n - \beta_n N_{\rm i}N_{\rm e})N_{\rm e} +$$
$$\frac{I}{h\nu}\sum_{n=0}^{M}\sigma_n N_n - \frac{dz_{\rm p}}{dt}\frac{N_{\rm e}}{z_{\rm p}} \quad (3)$$

$$\frac{dN_n}{dt} = \frac{d\mu_n}{dt}\frac{1}{Mz_{\rm p}} + \sum_{m=0}^{n-1}(k_{mn}N_m - r_{nm}N_n)N_{\rm e} -$$
$$\sum_{m=n+1}^{M}(k_{nm}N_n - r_{mn}N_m)N_{\rm e} - (\alpha_n N_n - \beta_n N_{\rm i}N_{\rm e})N_{\rm e} -$$
$$\frac{I}{h\nu}\sigma_n N_n - \frac{dz_{\rm p}}{dt}\frac{N_n}{z_{\rm p}} \quad (4)$$

$$\frac{dN_0}{dt} = \frac{d\mu_0}{dt}\frac{1}{Mz_{\rm p}} - \sum_{m=1}^{M}(k_{0m}N_0 - r_{m0}N_m)N_{\rm e} - (\alpha_0 N_0 -$$
$$\beta_0 N_{\rm i}N_{\rm e})N_{\rm e} - \frac{dz_{\rm p}}{dt}\frac{N_0}{z_{\rm p}} \quad (5)$$

$$\frac{dT_{\rm e}}{dt} = \frac{d\mu_{\rm e}}{dt}\frac{(T_{\rm s} - T_{\rm e})}{N_{\rm e}m_{\rm e}z_{\rm p}} - \frac{(T_{\rm e} - T_{\rm p})}{\tau_{\rm e}} -$$
$$\frac{2}{3N_{\rm e}}\sum_{n=0}^{M-1}\sum_{m=n+1}^{M}\Delta E_{nm}(k_{nm}N_n - r_{mn}N_m) -$$
$$\sum_{n=0}^{M}\left(\frac{2}{3}E_{\rm in} + T_{\rm e}\right)(\alpha_n N_n - \beta_n N_{\rm i}N_{\rm e}) +$$
$$\frac{I}{N_{\rm e}h\nu}\sum_{n=0}^{M}\left(\frac{2}{3}(h\nu - E_{\rm in}) - T_{\rm e}\right)\sigma_n N_n + \frac{2}{3}\frac{(I_{\rm abs} - I_{\rm em})}{N_{\rm e}z_{\rm p}} \quad (6)$$

$$\frac{dT_{\rm p}}{dt} = \frac{T_{\rm e} - T_{\rm p}}{\tau_{\rm e}} + \frac{\dfrac{d\mu}{dt}}{Mz_{\rm p}\left(N_0 + \displaystyle\sum_{n=1}^{M}N_n + N_{\rm i}\right)} \quad (7)$$

where k_{nm} and r_{nm} are the time constants for EI excitation and de-excitation processes, n is the electronic level of energy E_n,

α_n and β_n are the time constants for the ionization and recombination processes, E_{in} is the excited level ionization energy, ΔE_{nm} is the transition energy of the excited state ($n \rightarrow m$), I_{abs} is the laser irradiance absorbed by the vapor, I_{em} is the re-emitted intensity, z_p the height of the vapor cloud, h is the Planck constant, $h\upsilon$ is the incident laser photon, and σ_{nl} is the cross section for laser absorption by the excited species in the vapor.

In the present work, to calculate electron density and temperature, we individuated six Cu levels corresponding to the most intense nonresonant lines in the spectrum (3.8, 5.0, 5.4, 6.2, 7.7, and 8.8 eV). The population of such levels has been assumed as the sum of the levels next to them.

The vapor cloud is assumed to expand mainly along the normal to the target surface with sonic velocity

$$\frac{dz_p}{dt} = \sqrt{\frac{\gamma k_B T_p}{M}} \qquad (8)$$

where γ is the specific heat ratio. This approximation is effectively valid only in the first stages of plasma, and we used it only to take into account the plasma cooling due to its expansion.[29,30] The inclusion of a complete description of the hydrodynamic plasma expansion have been considered not relevant to the comparison with present experimental data collected in the early part of the expansion (time < 2 μs) where usually LTE is assumed.[31] For the same reason, the effect of nanoparticle mass ejection, mostly occurring at longer delays, has been neglected.[32]

We considered Bremsstrahlung emission as the main re-emission mechanism[25] in the laser-produced plasma, whose intensity is given by

$$I_{em} \cong 1.42 \times 10^{-34} T_e^{1/2} n_e^2 z_p \qquad (9)$$

2.1.2. Modeling LA with fs Pulses. The difference between the ablation process of ultrashort (<1 ps) and short (>10 ps and <100 ns) laser pulses relies on different mechanisms of energy dissipation in the target. In the case of longer-pulse irradiation, the material undergoes changes in its thermodynamic state from solid, through liquid, into a plasma state during the laser pulse, whereas in the case of ultrashort-laser-pulse irradiation, only a very hot electron gas and a practically undisturbed lattice are found at the end of the laser pulse.

In the latter case, the laser energy is first absorbed by the conduction band free electrons (Fermi electron gas) in the target; the deposited energy is very quickly equilibrated among the electrons through electron−electron scattering on the time order of a few to tens of femtoseconds,[33] and more slowly, it is transferred to the lattice through electron−phonon coupling on the order of picoseconds. The latter process is controlled by the strength of the electron−phonon coupling and can last from a fraction of picosecond to several tens of picoseconds as the electron−phonon energy transfer time is much longer than the femtosecond laser pulse duration. A state of thermal nonequilibrium is created in the target by laser irradiation, with electrons and the lattice having different temperatures. Only at later times is a thermal equilibrium established between the electrons and phonons, and the heat flow from the surface region into the bulk of the irradiated target can be described by the common thermal diffusion.

All of this implies that the femtosecond laser pulse interacts with a solid target with a power density remaining almost constant during the laser pulse. The major process occurring during the laser irradiation is the target electron heating by the laser field, but the laser will not be able to reheat the plasma as this is produced after the end of the pulse.

In order to describe the interaction of the electron and lattice subsystems with a femtosecond laser pulse, the two-temperature model is widely used.[34] The model accounts for the energy relaxation between electrons and phonons and the thermal diffusion, that is, Fourier law, as follows

$$\frac{\partial T_e}{\partial t} = \frac{\partial}{\partial x} D_e(T_e) \frac{\partial T_e}{\partial x} - \frac{T_e - T_p}{\tau_e(T_e)} + \frac{S(x,t)}{C_e(T_e)} \qquad (10a)$$

$$\frac{\partial T_p}{\partial t} = \frac{T_e - T_p}{\tau_p} \qquad (10b)$$

where C_e is the electron heat capacity, τ_e and τ_p are the electron and phonon relaxation times, and D_e is the electron thermal diffusivity.

As the heat capacity of electrons is about 2 orders of magnitude smaller than the one of a metal lattice,[35] the excited electrons in the target could be heated up to a very high temperature, while the lattice primarily remains thermally undisturbed. Due to the very small (in submicrometers) optical penetration (or skin) depth of metals, the gradient of the electron temperature could be very sharp. The final surface temperature is determined by a competition between electron−phonon coupling and hot electron diffusion in the target. Electron−phonon coupling will tend to localize the heat at the surface, whereas hot electron diffusion will result in heat transport away from the surface into the bulk.

This mechanism also explains the peculiar features observed for craters produced by differently lasting pulses.[36] In the case of the ultrashort pulse, the zone heated by the laser around its spot for heat diffusion is smaller, and the same has to be expected for the depth resolution. It is worth noting that longer laser pulses are able to deposit more energy into the solid. In order to remove an atom from a solid by means of a laser pulse, one should deliver energy in excess of the binding energy of that atom. Thus, to ablate the same amount of material with a shorter pulse, one should apply higher laser intensity (approximately in inverse proportion to the pulse duration.)

The two coupled eqs 10a and 10b, derived above, replace the previous eq 1 in describing the thermal diffusion properties of the target, while the following eqs 2−9 remain unchanged.

Our preliminary results, relevant to LA of the quaternary copper-based alloy, have been recently reported by R. Fantoni et al.,[37] showing that the proposed model approach still predicts fractionation, related to the long-lasting zinc evaporation, in the examined case.

The two-temperature approach, once introduced in the model presented for ns ablation, allows one to perform the same simulations and to compare predictions with experimental data obtained by means of fs pulses at different wavelengths and fluences.

2.2. Plasma Decay and LIBS Data Analysis. LIBS data analysis relies on processing of the intensity data of assigned atomic and ionic lines detected in suitable spectral and time-resolved windows. Different spectral windows were chosen for data acquisition of copper, tin, zinc, and lead lines possibly not

affected by saturation or self-absorption upon the selected experimental conditions. Namely, in UV LA experiments, Sn(I) lines at 270.65, 283.99, 286.33, 300.91, 303.41, and 326.23 nm were selected for temperature measurements and tin determination. Cu(I) lines at 296.12, 301.08, and 324.75 were selected for copper determination, a Pb(I) line at 287.50 nm was selected for lead determination, and a Zn(I) line at 334.50 nm was selected for zinc determination. In visible LA experiments, the Sn(I) line at 283.99 nm was considered for tin determination, Cu(I) lines at 282.43, 427.51, 465.11, 510.55, 570.02, and 578.21 nm were utilized for temperature measurements and copper determination, a Pb(I) line at 283.30 nm was used for lead determination, and a Zn(I) line at 472.21 nm was used for zinc determination. Physical parameters relevant to all of the spectral lines here utilized can be found in the NIST electronic database.[38]

In a laser-induced plasma, provided that radiative processes negligibly alter the balances of the collisional ones, the population density and plasma ionization are ruled by Boltzmann and Saha equilibrium relations.[39] This is the case of electron excitation kinetics driven plasma[5] in LTE conditions, which is characterized by only one thermodynamic temperature, that is, the electron temperature T_e. Following this assumption, the internal state density is governed by electrons, that is, the excitation, de-excitation, and ionization of heavy species present in the plasma (atoms and ions in different states) are dominated by electron collisions. The prevalence of electron-induced transitions implies that the particle number density n_j^p of species j and state p is given by Boltzmann statistic as in eq 11

$$\frac{n_{j,s}^p}{n_{j,s}^1} = \frac{g_{j,s}^p}{g_{j,s}^1} \exp[-(E_{j,s}^p - E_{j,s}^1)/k_B T_e] \quad (11)$$

in which the thermodynamic temperature is replaced by the electronic one T_e, k_B is the Boltzmann constant, $g_{j,s}^p$ and $g_{j,s}^1$ are the degeneracies of the considered states, and $E_{j,s}^p - E_{j,s}^1$ is the energy difference between excited state p and ground state 1. Similar considerations lead to the Saha conditions (eq 12) for atoms and ions in equilibrium, where the thermodynamical temperature is again substituted by the electron temperature

$$\frac{n_e n_{i,s}}{n_{a,s}^1} = 2\frac{U_{i,s}}{U_{a,s}}\frac{(2\pi m_e k_B T_e)^{3/2}}{h^3} \exp[-(E_s^\infty)/k_B T_e] \quad (12)$$

where n_e is the electron density, E_s^∞ is the effective ionization energy (whose value takes into account also its lowering due to plasma presence), and $U_{a,s}$ and $U_{i,s}$ are partition functions (eq 13) of atoms and ions

$$U_{j,s} = \sum_p g_{j,s}^p \exp(-E_{j,s}^p/k_B T_e) \quad (13)$$

A once assumed LTE condition, the temperature can be calculated through a Boltzmann plot for different species and at different delays after the end of the laser pulse. Knowing the plasma temperature, the electron densities can be calculated from Stark broadening[40] measured on selected well-resolved lines. The full width at half-maximum (fwhm) of a spectral line ($\Delta\lambda_{1/2}$) with the electron number density n_e is given by

$$\Delta\lambda_{1/2} = 2w\left(\frac{n_e}{10^{16}}\right) + 3.5A\left(\frac{n_e}{10^{16}}\right)^{1/4}[1 - 1.2n_D^{-1/3}]w\left(\frac{n_e}{10^{16}}\right) \quad (14)$$

where w is the electron impact parameter, A is the ion broadening parameter, and n_D is the number of particles in the Debye sphere. In the present analysis, only the first term has been utilized, with parameter values that can be found in the NIST electronic database.[38] The error in the determination of n_e by this method is $\sim20-30\%$. Electron density data were obtained by Stark broadening of the Pb(I) 280.4 nm emission line originating at 3.82 eV for sample S6 in the UV (0.027 nm @ $N_e = 10^{17}$ cm^{-3})[41] and on the Cu(I) 510.55 nm line originating at 5.74 eV for the Hi−Pb sample in the green (0.014 nm @ $N_e = 10^{17}$ cm^{-3}).[42] It is worth reminding here that the necessary condition to assess the lower limit for the electron density at which the plasma is still assumed to be in LTE is given, according to H. C. Liu et al.,[31] by

$$N_e \text{ (cm}^{-3}) \geq 1.4 \times 10^{14}[T \text{ (eV)}]^{1/2}[\Delta E \text{ (eV)}]^3 \quad (15)$$

where ΔE is the largest energy transition for which the condition holds and T is the temperature. This lower limit of N_e is about 2×10^{16} cm^{-3} for the considered Cu lines.

The onset of LTE in the time windows selected for all data acquisition, except for kinetic measurements, has been checked on the listed tin lines in the case of UV experiments and on copper lines in the case of green LA. Similar equilibrium temperatures (around 7000 K) were obtained from the slopes of the respective Boltzmann plots (eq 11). Within the same time windows, the measured electron density value was high enough to assume LTE and also low enough (of the order of 10^{17} cm^{-3}) to ensure that the contribution of ionic states to the total intensity, used to retrieve major constituent concentrations, was negligible (less than 1% for each element), as in the previous cases reported by A. Elhassan et al.[18] and A. De Giacomo et al.[22]

3. Experimental Section

3.1. fs and ns LIBS Setups. Experimental data, here reported to validate the model and to understand the limits of LIBS analytical application to copper-based alloys, related both to the nature of the sample (matrix effect) and to the choice of experimental parameters (in the attempt to minimize fractionation), have been collected with four different setups, adopting, as much as possible, a similar geometrical arrangement placing the collecting detection system along the main expansion direction of the generated plasma and at 45° from the target surface. The different LIBS setups are reported in A. Elhassan,[18] F. Colao et al.,[19] and A. De Giacomo et al.[22]

Data in the UV at 248 nm have been collected at FORTH, Iraklion (GR), by using existing excimer laser fs and ns facilities (500 fs and 15 ns pulse durations, respectively) with a LIBS setup based on a low-resolution monochromator coupled to an ICCD. The ns source was operated at energies of 14.2 and 10.5 mJ focused on a spot sizes of 1.5×10^{-4} and 4.5×10^{-4} cm^2, respectively; the fs source was operated at energies of 11.0 and 8.2 mJ focused on a spot size of 1.3×10^{-3} cm^2. A complete description of the experiments, together with more data collected at the highest energies, can be found in A. Elhassan et al.[18]

A Nd/glass laser source, operating in second harmonic at 527 nm, emitting 250 fs pulses, has been utilized at the Basilicata University (Potenza) to collect data in the visible region. The

Modeling of Laser Ablation of Quaternary Bronze Alloys

J. Phys. Chem. A, Vol. 113, No. 52, 2009 **14369**

fs source was operated at energies of 3.0 and 0.75 mJ focused on a spot size of 2.0×10^{-4} cm². The respective LIBS setup based on a high-resolution monochromator coupled to an ICCD is described in A. De Giacomo et al.,[22] where some results on different copper-based alloys containing also nickel are reported. Visible ns pulse ablation experiments have been performed at ENEA-Frascati by using a Nd:YAG system operated in second harmonic at 532 nm, emitting 8 ns pulses. The ns source was operated at energies of 29 and 9 mJ focused on a spot size of 2.0×10^{-3} cm². The high-resolution LIBS setup previously described in F. Colao et al.[19] was utilized.

In all experiments, spectra have been recorded on ICCD detectors with a time resolution on the order of 10 ns or better, sufficient to control the gate parameter (delay and width) in the range of interest (100−10000 ns). Unless differently specified in the text during kinetic measurements, typical gate delays and widths were utilized during the LIBS data acquisition in combination with each laser source. Namely, the gate delay and width were 900 ns upon nanosecond UV irradiation and 100 or 300 ns with a 300 ns width for femtosecond UV irradiation; in the visible region, the delay and width were fixed at 1000 ns for nanosecond pulses and 400 or 100 ns with a 2500 ns width for femtosecond pulses.

A normalization method has been exploited to avoid any unwanted experimental fluctuations. Lines used for normalization have been selected according to the following features:

• They are located in the same region of the lines under investigation to avoid any possible nonlinearity in the detection system.

• They are characterized by high lower-energy levels and small transition probabilities, which strongly lower the possibility of its self-absorption in the colder parts of the plasma.

• They are well-resolved lines and not affected by any interference with other spectral lines.

3.2. Copper-Based Alloy Samples. Experiments have been performed on different alloys containing mainly copper (about 80% or more) and, as additional elements, two or three of the following metals, Sn, Zn, and Pb. The presence of lead in the selected samples was considered for the interest in its determination on ancient artifacts.[43]

The sample concentration was known from synthesis of the alloys and independently tested by X-ray fluorescence (XRF) in most cases. Samples utilized in the fs/ns comparison were the same for each series of experiments performed at the same laser wavelength; the respective compositions are listed in Table 1a and b. Data reported in the table refer to the sample synthesis (nominal values) and are therefore reported without experimental error bars; measured XRF data resulted in agreement, with an expectation of better than 1% in all examined cases, macroscopic agreement being better than 0.1% due to the synthesis process itself.

In order to optimize the signal-to-noise ratio and spectra reproducibility, the detection of LIBS spectra was carried out by averaging seven single measures in three different positions of the sample in the UV experiments.

For the same reason, for green fs and ns pulses, all acquisitions were integrated over 50 or 100 shots focused onto the target positioned on a rotating holder (1.2 rpm speed), exposing a new surface to each couple of successive laser pulses. Data collected with ns pulses have been filtered by using the algorithm described in V. Lazic et al.;[44] the averaged number of pulses has been 50 at least.

3.3. The Internal Standardization (IS) Method. LIBS quantitative analysis requires one to fully understand to what

TABLE 1: Elemental Composition in %wt/wt of Quaternary and Ternary Certified Copper Based Alloys

sample code	Cu (%)	Sn (%)	Zn(%)	Pb(%)
(a) Samples Utilized for LA Experiment upon Ultraviolet Irradiation at 248 nm				
S1	80.00	5.00	0.00	15.00
S2	90.00	6.00	0.00	4.00
S3	92.30	7.50	0.00	0.20
S4	82.30	3.00	14.00	0.50
S5	87.30	6.30	3.70	2.70
S6	83.82	5.487	4.50	5.66
E	95.17	4.00	1.11	0.00
G	90.83	7.17	1.75	0.00
H	87.10	1.92	10.83	0.00
(b) Samples Utilized for LA Experiment upon Visible Irradiation near 530 nm.				
B3	80.25	12.96	2.27	1.65
B4	84.00	11.05	1.22	2.50
B22	82.75	3.85	4.40	6.12
B21	83.05	5.13	6.17	3.79
Hi−Pb	82.40	5.30	5.90	5.60
Lo−Pb	88.20	9.80	0.47	0.77

extent the elemental plasma stoichiometry, as it emerges from line intensity measurements, corresponds to the actual surface composition. Plasma emission depends not only on laser parameters and geometry, which have to be optimized in each individual case, but also on composition, surface condition, and thermal properties of the sample. The latter are known as matrix effects and affect the line intensity of an element embedded in a particular matrix. To avoid a number of experimental parameters that are difficult to measure, the so-called internal standardization method has been proposed and widely used. The method is based on the following principle; a number of reference samples are prepared, all having a similar and known elemental composition. Usually, in such a set of samples, a suitable element dominates as the internal standard and defines the sample properties in view of the matrix effects. It is, therefore, expected that plasma emission be less affected from sample to sample. In a LIBS experiment, the ratio of the line intensity of a trace element to the emission line of the internal standard is measured and plotted as a function of the known concentration ratios in the reference samples.[45] These plots are the calibration curves that allow quantitative analysis in unknown samples. Obviously, a limit is set to the applicability of this method because a similar composition for the unknown sample is also required. A large number of data based on this method have shown that this can be anticipated for laboratory measurements, where reference and unknown samples can be embedded in similar matrixes, but it is a severe restriction for field experiments where the sample composition is unknown.

However, copper-based alloys here examined in a given range of copper concentrations (>80%) seems to fulfill the requirement of a homogeneous matrix, which, in principle, supports the use of calibration curves.

4. Results and Discussion

In this part, model simulations are compared with experimental data collected at two different fluences for each wavelength utilized to induce LA by fs or ns laser pulses on all the examined copper based alloys.

In the following, the model results are reported and discussed in order to clarify the role of selected experimental parameters on the ablation process and on the assumption of LTE for subsequent LIBS analysis (section 4.1). An attempt to relate

the effects of better understanding of these fundamental aspects on the analytical figures of merit relevant to quantitative analysis is presented in section 4.2, and the comparison is limited of course to those quantities which can be both predicted and measured with the available tools.

4.1. Thermodynamics of the Process. *4.1.1. Vaporization Mechanism and Fractionation.* In order to understand how our LA model can take into account fractionation, before discussing results any further, we have to define a parameter which is able to quantify fractionation in LIBS analysis. In M.E. Taylor et al.,[9] fractionation from the original sample to the laser-induced plume is independently measured for each element on the film collected onto a nearby substrate in a pulsed laser deposition experiment. According to M.E. Taylor et al.,[9] fractionation can be expressed as a ratio, $R_1 = (C_F - C_{Cert})/C_{Cert}$, where C_F is the element concentration in the deposited film and C_{Cert} is the same known element concentration in the target. In our case, we cannot either measure or calculate C_F, but we may assume that C_F is the element concentration in the plume, either calculated by our model or measured by LIBS from the intensity of a selected line. Note that for each considered element, the R_1 value is zero in the absence of fractionation, $|R_1| > 0.1$ is considered an indication of appreciable fractionation according to M. E. Taylor et al.,[9] and the sign of R_1 carries information about the tendency to a fractionation richer or poorer in that element in the vapor phase.

Preliminary model simulations of a quaternary bronze alloy LA (Lo−Pb sample) at about 530 nm have been already reported in R. Fantoni et al.,[37] showing an anomalous Zn evaporation, which, in the investigated parameter range (150 J/cm², 250 fs), does depend on the laser fluence and proceeds much longer than the pulse duration. An even larger effect was generated upon irradiation with ns pulses.[37] The effect of plasma enrichment in zinc is enhanced during the cooling down of the target as this process is slower than the heating one. The surface, heated by laser irradiation through fast electron−phonon coupling, gradually thermalizes, in fact, with the bulk through slower phonon diffusion.

Since upon ns LA the model already predicted a reduction of fractionation when going from 1064 to 355 nm,[16] the benefit of using a wavelength deeper in the UV has been tested both with ns and fs pulse durations.

Results of the current model simulations performed by varying one laser parameter at a time for the Hi−Pb sample are shown in Figure 1, where the chosen reference settings are 530 nm wavelength (λ), 15 J/cm² fluence (ϕ), and 8 ns pulse duration (τ). Note that the fractionation index here reported is defined as $R_1 = (C_{th} - C_{cert})/C_{cert}$, where C_{th} is the simulation outcome for each element plasma concentration and C_{cert} is the corresponding certified value in the considered sample. Data reported in the figure confirm, quantitatively, formerly observed fractionation effects for copper-based alloys and their progressive reduction with increasing fluence (Figure 1a) and decreasing wavelength (Figure 1b). Decreasing pulse duration originates a reduction of fractionation only above 10 ns; conversely beneficial effects in further shortening the pulse duration from a few ns to hundreds of fs are not expected (Figure 1c).

4.1.2. Plasma parameters. Once verified the occurrence of LTE, isolated atomic lines free from saturation and self-absorption were utilized to construct a Boltzmann plot for temperature retrieval. As already mentioned, tin lines were used in the UV experiments and copper lines in the visible ones.

Stark broadening of spectral lines was used to determine the plasma electron density, as reported in section 2.2. Beside Stark
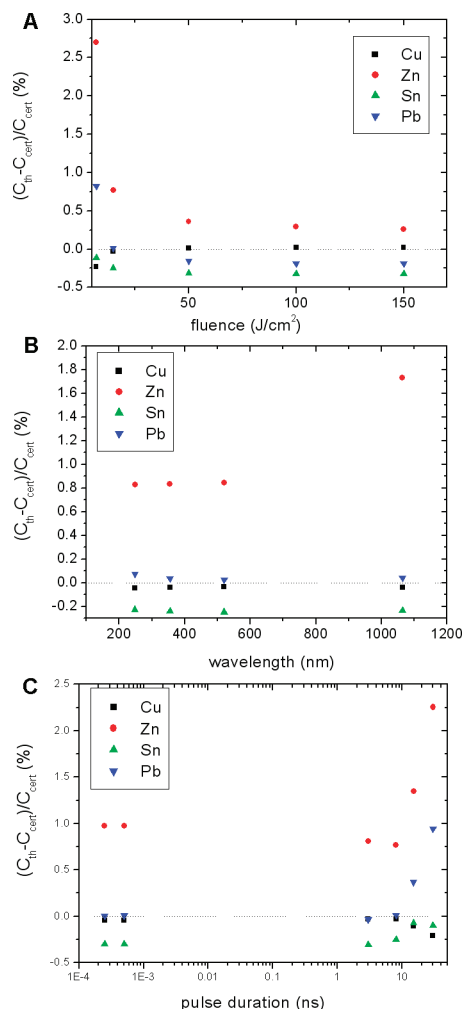

Figure 1. Model calculations of fractionation ratio R_1 during the LA process as a function of different laser parameters, (a) fluence, (b) wavelength, and (c) pulse duration. Hi−Pb sample fixed laser parameter settings are, in turn, couples among $\phi = 15$ J/cm², $\lambda = 530$ nm, $\tau = 8$ ns.

broadening, there are many other broadening mechanisms which simultaneously take place during LIBS signal generation (e.g., Doppler broadening, pressure broadening by collisions with foreign species, resonance broadening) and depend both on the chosen line and on the experimental parameters. Thus, it is neither trivial nor an easy task to take all of these factors into account and calculate what would be the emission escaping from the plasma and how it is related to plasma characteristics. The rough approximation to consider only the Stark effect as responsible of the measured broadening leads to values of electron densities which are very likely systematically overestimated but are affected in the same way by all other experimental parameters different from the laser pulse characteristics. A comparison with theoretical prediction can, therefore, be useful to understand and confirm increasing or decreasing trends.

Average temperatures and electron densities calculated from our models are reported in Table 2. Theoretical data are compared with the corresponding experimental ones in Table 2a, while the effect of varying either the laser wavelength or the pulse duration at the same fluence is shown in Table 2b for fs LA. The comparison shows a reasonable agreement for the absolute values of both plasma parameters (within an order of magnitude) and a good agreement in the trend as experimental

TABLE 2: Calculation of Plasma Parameters[a] Table 2 (a)

(a) Comparison between Average Experimental and Theoretical Values of Plasma Temperature and Electron Density Calculated in the Time Windows Reported in Parentheses

pulse duration @ irradiation wavelength (gate delay - width)	ϕ (J/cm^2)	T (K)		$N_e \times 10^{17}$ (cm^{-3})	
		exp	theory	exp	theory
ns @ 248 nm (500−900 ns)	93	7900 ± 400	9900 ± 300	9.3 ± 1.3	12 ± 2
	13	7500 ± 400	9400 ± 300	8.7 ± 1.3	9 ± 2
fs @ 248 nm (500−900 ns)	8.7	6800 ± 300	7200 ± 100	5.4 ± 0.6	1.1 ± 0.1
	6.5	6400 ± 300	7200 ± 100	4.6 ± 0.6	1.0 ± 0.1
ns @ 532 nm (400−1750 ns)	15	9600 ± 600	9600 ± 300	6.1 ± 0.8	8.7 ± 2
fs @ 527 nm (400−1750 ns)	15	7700 ± 300	7300 ± 150	4.0 ± 0.7	1.2 ± 0.4

(b) Theoretical Values of Plasma Temperature and Electron Density Calculated at the Given Experimental Parameters for fs LA

detection time range	λ (nm)	τ (fs)	ϕ (J/cm^2)	T (K) theory	$N_e \times 10^{17}$ (cm^{-3}) theory
(400−1750) ns	248	250	15	7300 ± 100	1.3 ± 0.1
(400−1750) ns	520	250	15	7300 ± 100	1.3 ± 0.1
(400−1750) ns	248	500	15	6600 ± 100	0.29 ± 0.01
(400−1750) ns	520	500	15	6600 ± 100	0.29 ± 0.01

[a] Averaged values have been calculated in the gate window reported in parentheses where LTE has been assumed.

TABLE 3: Comparison between Average Experimental and Theoretical Values of Plasma Temperature and Electron Density Decay, As Calculated in the Respective LTE Windows (reported in parentheses)

pulse duration @ irradiation wavelength (gate delay - width)	ϕ (J/cm^2)	exponential decay time of T (ns)		exponential decay time of N_e (ns)	
		exp	theory	exp	theory
ns @ 248 nm (500−900 ns)	93	534 ± 300	893 ± 10	466 ± 200	424 ± 10
	13	1220 ± 300	1140 ± 10	454 ± 200	422 ± 10
fs @ 248 nm (500−900 ns)	8.7	302 ± 70	340 ± 20	216 ± 150	133 ± 20
	6.5	179 ± 20	300 ± 20	130 ± 50	142 ± 20
ns @ 532 nm (400−1750 ns)	15	965 ± 200	798 ± 10	366 ± 80	414 ± 10
fs @ 527 nm (400−1750 ns)	15	990 ± 250	900 ± 5	502 ± 150	454 ± 5

parameters were changed. Since one of the basic assumptions of the model is the occurrence of LTE in the plasma,[15] present results support this occurrence for the data collected in the considered temporal range. The range of electron density values coming from the simulation is, however, larger than the measured ones. In more detail, results of calculations reported in Table 2b show that, in the investigated range of hundreds of fs and for wavelengths in the visible−UV range, with a variation of a factor of two in either the wavelength or pulse duration, the model predicts a larger dependence from the latter for both parameters. In particular, the shortening of the laser pulse corresponds to an increase on the order of 10% in temperature and of a factor four in electron density. The latter plasma parameter results are by far the most sensitive to the ablating pulse duration. In fact, by increasing laser power, that is, decreasing the pulse length, the temperature gradient in the sample is increased together with the surface temperature. Higher surface temperature induces faster material evaporation at the surface, according to eq 2a; therefore, more material contributes to plasma formation. Our model predicts, with the considered experimental parameters, that by doubling the laser pulse duration, the target melting depth is reduced to 1/5, the maximum surface temperature rate of change is reduced to 2/3, and the surface remains at a temperature higher than the melting point for a period of five times shorter.

4.1.3. Plasma Kinetics. The time evolution of plasma parameters has been investigated by varying the data acquisition delay time from 100 ns after the laser pulse, in steps of 100 ns with the same gate width (100 ns). Within the LTE window appropriate to each set of experiments, a single exponential decay was assumed for both plasma parameters, and the corresponding time constants were retrieved after deconvolution

of the laser pulse Gaussian profile. Experimental and theoretical results are compared in Table 3 at the examined wavelengths and fluences.

Both parameters show the same trend, although temperature appears more sensitive to laser fluence variations. Nevertheless, experimental error bars are rather large; significantly shorter decay constants have been obtained when going from ns to fs LA at comparable laser fluences in the UV range. The effect is confirmed by theoretical calculations which reproduce well, also, the larger decay constants observed after fs LA in the visible with respect to the UV at a comparable fluence.

Besides plasma parameter evolution, the kinetics of selected copper lines have been investigated in order to complete the characterization of plasma dynamics and further check the onset of LTE in the time window chosen for the analytical determination in each experiment. Results are reported in Figure 2 for fs (a) and ns (b) LA at the considered wavelengths. Levels at different initial energies have been selected with the purpose to look for the occurrence of different decay constants. The latter parameters, as retrieved from experimental data assuming a single exponential decay in the investigated time window, are reported in Table 4.

In agreement with the simulations, experimental data obtained in the investigated LTE window show single exponential decay; the respective decay constants depend on the initial level value and on the laser pulse duration. In particular, values twice longer are obtained experimentally in passing from fs to ns irradiation at the same wavelength and fluence. The dependence on wavelength and fluence of the decay constants has been separately investigated in the IR upon ns irradiation at 1064 nm, and no significant difference has been obtained in the
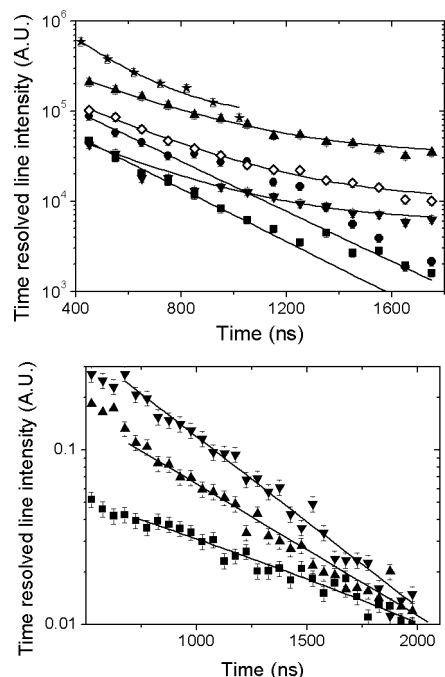
Figure 2. Kinetics of main Cu emission lines examined; (top) fs laser irradiation at $\phi = 15$ J/cm^2 with $\lambda = 527$ nm (lines: ■ 427.51 nm, ● 465.11 nm, ▲ 510.55 nm, ▼ 570.02 nm, ◇ 578.21 nm) and $\phi = 6.5$ J/cm^2 with $\lambda = 248$ nm (line: ★ 296.12 nm); (bottom) ns laser irradiation at $\phi = 15$ J/cm^2 with $\lambda = 534$ nm (lines: ▲ 296.14 nm, ■ 427.51 nm, ▼ 570.02 nm) performed on a HiPb sample. Full lines are best fits of single exponential decay.

TABLE 4: Theoretical and Experimental Decay Constants Obtained for Different Cu Lines in Bronze LA Performed with ns and fs Laser Sources Operated Either in the Green or in the UV, the Latter Marked by * (See Figure 3 for the Range Utilized in the Respective Fit and for Sample Specification)

Cu(I) lines wavelength (nm)	E_k (cm^{-1})	theory (fs)	exp (fs)	theory (ns)	exp (ns)
296.12	44963	248 ± 8*	202 ± 12*	508 ± 8	570 ± 50
427.51	62403	315 ± 8	296 ± 13	440 ± 8	444 ± 45
465.11	62403	315 ± 8	312 ± 19	440 ± 8	480 ± 50
510.55	30783	327 ± 8	373 ± 12	490 ± 8	740 ± 75
570.02	30783	327 ± 8	346 ± 10	490 ± 8	1080 ± 100
578.21	30566	341 ± 8	341 ± 11	505 ± 8	920 ± 90

selected Cu(I) lines for all of the investigated fluences range (ϕ varying from 10 to 100 J/cm^2; data not shown).

In Table 4, theoretical values for the decay constants are reported for comparison; as clustering occurs, the copper levels used in the theoretical model around six selected energies (3.8, 5.0, 5.4, 6.2, 7.7, and 8.8 eV) are assumed to be populated with the available electron densities. The dependence of the decay constant on the upper energy level is confirmed by the model within the estimated error bars, although experimental variations appear slightly larger.

4.2. Analytical Figures of Merit. *4.2.1. Calibration Curves.* Calibration curves are constructed by plotting the maximum line intensities of selected analytical lines as a function of the percentage weight composition (%wt/wt) of the analyte in the alloy. In order to minimize fluctuations that arise from matrix effects and from laser instability, the analyte emission was normalized with respect to the emission from Cu(I), the major element of the alloy for both UV (Figure 3) and green visible (Figure 4) LA.

Figure 3 shows the lines obtained by fitting experimental data to intensity ratios after scaling the respective theoretical calibra-
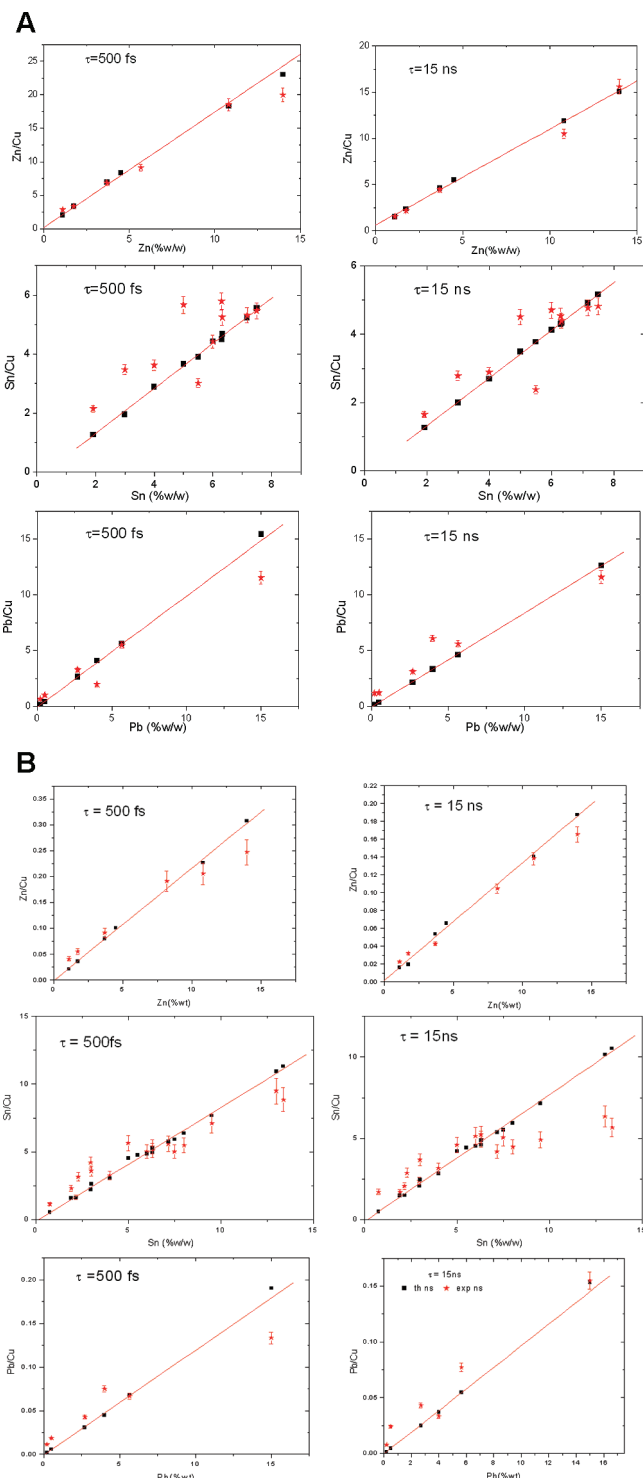

Figure 3. Comparison of calibration curves; (A) theoretical (■) and normalized experimental (★) calibration graphs for femtosecond (left) and nanosecond (right) laser irradiation obtained at $\lambda = 248$ nm with $\phi = 93$ and 8.7 J/cm^2, respectively; (B) theoretical (■) and normalized experimental (★) calibration graphs for femtosecond (left) and nanosecond (right) laser irradiation obtained at $\lambda = 248$ nm with $\phi = 13$ and 6.5 J/cm^2, respectively.

tion coefficients. Figure 3a reports the comparison between the calibration lines at high fluence both for nanosecond ($\phi = 93$ J/cm^2) and femtosecond ($\phi = 8.7$ J/cm^2) laser irradiation, while Figure 3b shows results obtained at the lower fluences ($\phi = 13.0$ and 6.5 J/cm^2, respectively). In the case of zinc, it is possible to observe that the experimental and theoretical

Modeling of Laser Ablation of Quaternary Bronze Alloys

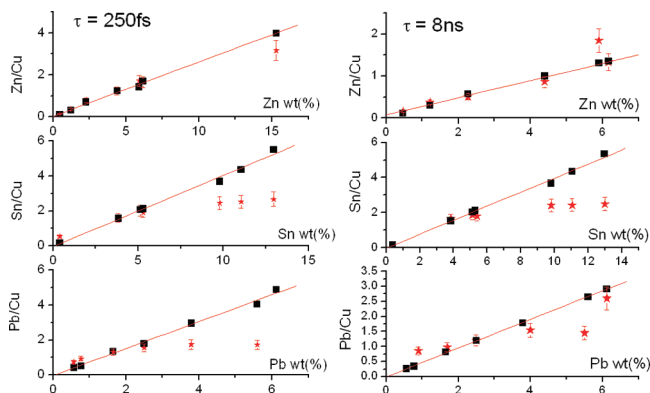*J. Phys. Chem. A, Vol. 113, No. 52, 2009* **14373**

Figure 4. Theoretical (■) and normalized experimental (★) calibration graphs for femtosecond (left) and nanosecond (right) laser irradiation at $\lambda = 527$ and 532 nm obtained with $\phi = 15.0$ J/cm^2.
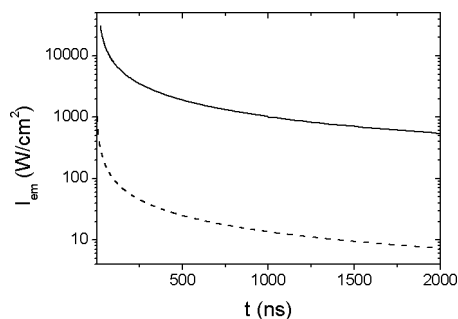

Figure 5. Green LA: Calculated reemitted light from plasma due to Bremsstrahlung radiation for 8 ns and 250 fs laser irradiation both at $\phi = 15$ J/cm^2 for the HiPb sample, reported as a function of the time after the laser pulse.

calibration graphs clearly exhibit the same change of slope in passing from femtosecond to nanosecond laser irradiation.

Similar results have been obtained in Figure 4 with the green irradiation at a fluence comparable to the lowest cases in the UV. It is worth noticing that in both cases, the Zn calibration curve is quite satisfactory in all of the large concentration range investigated, whereas for Pb, a deviation from linearity is encountered for lead concentrations larger than 4%. The disagreement, observed irrespective of the use of fs or ns sources, might be related to the tendency of lead to cluster in grains instead of forming homogeneous alloys, which might affect the experimental determination in different surface points. To a minor extent, deviations are also observed for tin at fluences equal to or lower than 15 J/cm^2, which confirms results previously obtained at different wavelengths (1064 and 355 nm) with ns pulses,[15,16] thus indicating that convergence toward a stoichiometric evaporation for bronzes is approached only at the highest fluence examined.

The validation of theoretical data by the experimental results may help to have a better understanding of the process and to more accurately relate LIBS experimental analysis to the real sample stoichiometry. In the analyzed cases, no remarkable influence is observed on the fractionation process by using either of the different laser pulse durations examined. The same conclusion can be drawn from both theoretical and experimental data.

4.2.2. LOD Optimization. The light re-emitted by the plasma due to Bremsstrahlung radiation has been calculated according to Y. B. Zel'dovich and Y. P. Raizer,[22] and the results are shown in Figure 5. It is remarkable that the Bremsstrahlung radiation has lower intensity and decreases more rapidly with time after fs laser irradiation as compared to that after the ns one. This fact, to be related to an increase in signal-to-noise ratio, could

improve the elemental detection limit in LIBS analysis with fs laser irradiation.

The higher sensitivity in minor element determination achievable by fs LA with respect to ns LA is also confirmed by the slope steeper by a factor two observed on calibration curves for Zn calculated at the same fluence ($\phi = 15$ J/cm^2), namely, 0.258 ± 0.007 for fs versu 0.112 ± 0.002 for ns (data in Figure 4).

4.2.3. Accuracy of Concentration Measurements. The accuracy of LIBS concentrations retrieved from the line intensity indeed relies on temperature measurements. This can be demonstrated by differentiating the usual equation relating the LIBS line intensity to a species concentration N for the respective transition (from eqs 11 and 12). Provided that a weak dependence of the partition function $U(T)$ versus the temperature can be assumed, for example, $\partial U(T)/\partial T \ll (U(T)/T)(E_{ki}/kT)$ (as usual for metals below 10000 K),[46] the approximate expression for the variation of concentration $\delta N/N$ versus temperature changes $\delta T/T$ gives numbers larger than 1. In particular, for the resonant copper lines at 3.8 eV and a temperature of 8000 K, we estimate $(\delta N/N)/(\delta T/T) = 4$, which means that a more accurate temperature determination results in a four time improvement of the accuracy in the retrieved concentration.

As can be inferred from the results of simulation of plasma parameters reported in Table 2, the calculated uncertainty in temperature is smaller for fs LA than that for ns LA, namely, a factor of 3 at 248 nm and a factor of 2 at around 530 nm; thus, we expected a corresponding increase in the accuracy of concentration determination going from ns to fs pulse irradiation.

It is worth noticing that the experimental findings reported in Table 2 show a smaller improvement in the accuracy going from ns to fs irradiation; this can be attributed partially to the smaller stability and greater complexity of the experimental fs setup. Another explanation might be related to the decay times for fs ablation with UV irradiation, which are shorter than those for the case of ns irradiation (see Table 3); the time window for LTE is accordingly shortened, thus resulting in higher statistical errors because of the decrease of the number of data available for computation of parameters.

5. Conclusions

Results reported in the present paper show that the proposed model for LA is suitable to describe the vaporization of ternary and quaternary copper-based alloys formed by Cu, Sn, Zn, and Pb in a concentration range of interest for Cultural Heritage material characterization (copper concentration > 80%). The model, in which a two-temperature approach has been introduced to take into account the initial dynamics upon ultrashort laser irradiation, is capable of justifying the shorter plasma duration upon fs ablation and the lower fractionation observed for some set of laser parameters.

Concerning plasma kinetics of both main plasma parameters, the model is suitable to reproduce their absolute values and to simulate their time evolution; for the temperature absolute value, the agreement is within the experimental error bar, while for the electron density, it is within a factor of 4 or better. This is of special relevance to LIBS implementation since these plasma parameters are utilized in retrieving analytical data in calibration-free procedures,[24] once LTE is assumed in the detection time window. The observed agreement on electron density further supports the latter assumption in the selected temporal windows.

Kinetics analysis of Cu line emission from different average levels of irradiation allowed further tests of the validity of the LTE assumption. In particular, the decay constants obtained with

14374 *J. Phys. Chem. A, Vol. 113, No. 52, 2009*

Fornarini et al.

a single exponential fit support the validity of this assumption for the Cu(I) lines selected in a broad energy range, where the energy of the upper level considered determines only the absolute value of the time constant obtained in the considered time window. Similar trends, theoretically predicted by the model, are observed both for ns and fs irradiation. We observed for the first time that the respective values do depend on the pulse duration, varied by 3 orders of magnitude, but are rather insensitive to the other laser parameters which, however, were varied on small scales (about 1 order of magnitude for the fluence and a factor of 4 for the wavelength).

In conclusion, the residual fractionation occurring especially at low laser fluences both for fs and ns LA appears more related to the ablation process itself than to deviation from LTE in the range of laser parameters here considered, and the utilization of pLTE, proposed in De Giacomo et al.,[22] seems not necessary in the investigated time windows for the examined alloys composition.

According to the model, the irradiation wavelength and pulse duration affect the stoichiometry of evaporation to a minor extent compared to that of the total fluence. The use of shortest wavelengths (UV and green) with respect to the IR ones seems to be mostly supported by a larger ablation efficiency, which might lead to an improvement in the statistics.

In agreement with model predictions, the normalization of the line intensity of components different from Cu to the one of copper permits one to build linear calibration curves, provided that the concentration range of all other elements maintains a copper matrix where the Cu concentration is around 80% or larger. The linearity is observed in all cases for experimental curves relevant to Zn, while deviation for Pb and Sn are observed as their concentrations exceed 3 and 8%, respectively, at laser fluences lower than 15 J/cm^2, irrespective of the pulse duration and the laser wavelength in the examined range (250 fs−15 ns; 248−527 nm).

The residual matrix effect observed in fs LIBS on copper-based alloys at both of the examined wavelengths, although less dramatic than that in former IR LA,[15] is still limiting the accuracy of the analytical results obtained and requiring the use of different calibration curves for different ranges of compositions corresponding to a different kind of copper-based alloys, that is, to really a different matrix. The only alternative is to follow a calibration-free approach, with proper assumption on LTE, which is expected to give satisfactory analytical results only in the presence of a few known components.[22]

However, the predicted improvement in signal-to-background ratio and in concentration accuracy related to temperature determination, together with the observed steepest calibration curve slope for minor element detection (such as zinc), can be considered as definite advantages of fs LIBS, which may compensate the larger complexity of the set-up and support its analytical utilization.

References and Notes

(1) Russo, R. E.; Mao, X.; Liu, H.; Gonzalez, J.; Mao, S. S. *Talanta* **2002**, *57*, 425–451.

(2) Choi, Y. S.; Lee, S. C.; Im, H. S.; Park, C. J. *Microchem. J.* **1999**, *63*, 24–33.

(3) Miziolek, A. W., Schechter, I., Palleschi, V., Eds. *Laser-Induced Breakdown Spectroscopy (LIBS): Fundamentals and Applications*; Cambridge University Press: Cambridge, U.K., 2006; ISBN-13: 9780521852746.

(4) Fryer, B. J.; Jackson, S. E.; Longerich, H. P. *Can. Mineral.* **1995**, *33*, 303–312.

(5) Vorob'ev, V. S. *Phys. Usp.* **1993**, *36*, 1129–1157.

(6) Kroslakova, I.; Günther, D. *J. Anal. At. Spectrom.* **2007**, *22*, 51–62.

(7) Kuhn, H.-R.; Günther, D. *Anal. Chem.* **2003**, *75*, 747–753.

(8) Borisov, O. V.; Mao, X. L.; Fernandez, A.; Caetano, M.; Russo, R. E. *Spectrochim. Acta, Part B* **1999**, *54*, 1351–1365.

(9) Taylor, M. E.; Blaney, D. L.; Cardell, G. *Appl. Surf. Sci.* **2000**, *165*, 166–177.

(10) Le Drogoff, B.; Margot, J.; Vidal, F.; Laville, S.; Chaker, M.; Sabsabi, M.; Johnston, T. W.; Barthélemy, O. *Plasma Sources Sci. Technol.* **2004**, *13*, 223–230.

(11) Le Drogoff, B.; Chaker, M.; Margot, J.; Sabsabi, M.; Barthélemy, O.; Johnston, T. W.; Laville, S.; Vidal, F. *Appl. Spectrosc.* **2004**, *58*, 122–129.

(12) Bleiner, D.; Chen, Z.; Autrique, D.; Bogaerts, A. *J. Anal. At. Spectrom.* **2006**, *21*, 910–921.

(13) Ershov-Pavlov, E.; Catsalap, K.; Rozantsev, V.; Stankevich, Yu.; Stepanov, K. *Emission spectra of laser induced plasmas at the elemental analysis of solids, measurement and modeling results*; VI Serbian−Belarusian Symposium on Phys. and Diagn. of Lab. & Astrophys. Plasma, Belgrade, Serbia, 2007; Vol. 82, pp 83−100.

(14) Capitelli, M.; Armenise, I.; Bruno, D.; Cacciatore, M.; Celiberto, R.; Colonna, G.; De Pascale, O.; Diomede, P.; Esposito, F.; Gorse, C.; Hassouni, K.; Laricchiuta, A.; Longo, S.; Pagano, D.; Pietanza, D.; Rutigliano, M. *Plasma Sources Sci. Technol.* **2007**, *16*, S30–S44.

(15) Fornarini, L.; Colao, F.; Fantoni, R.; Lazic, V.; Spizzichino, V. *Spectrochim. Acta, Part B* **2005**, *60*, 1186–1201.

(16) Fornarini, L.; Spizzichino, V.; Colao, F.; Fantoni, R.; Lazic, V. *Anal. Bioanal. Chem.* **2006**, *385*, 272–280.

(17) Margetic, V.; Pakulev, A.; Stockhaus, A.; Bolshov, M.; Niemax, K.; Hergenröder, R. *Spectrochim. Acta, Part B* **2000**, *55*, 1771–1785.

(18) Elhassan, A.; Giakoumaki, A.; Anglos, D.; Ingo, G. M.; Robbiola, L.; Harith, M. A. *Spectrochim. Acta, Part B* **2008**, *63*, 504–511.

(19) Colao, F.; Fantoni, R.; Lazic V. LIPS as an analytical technique in non-equilibrium plasma. In Ochkin, V., Ed.; *SPIE Special Issue on Spectroscopy of non equilibrium plasma at elevated pressures*; SPIE: Bellinghan, WA, 2002; Vol. 4460, pp 339−348.

(20) Galmed, A. H.; Harith, M. A. *Appl. Phys. B: Laser Opt.* **2008**, *91*, 651–660.

(21) Amoruso, S.; Bruzzese, R.; Spinelli, N.; Velotta, R. *J. Phys. B* **1999**, *32*, 131–172.

(22) De Giacomo, A.; Dell'Aglio, M.; De Pascale, O.; Gaudiuso, R.; Teghil, R.; Santagata, A.; Parisi, G. *Appl. Surf. Sci.* **2007**, *19*, 7677–7681.

(23) Lazic, V.; Barbini, R.; Colao, F.; Fantoni, R.; Palucci, A. *Spectrochim. Acta, Part B* **2001**, *56*, 807–820.

(24) Corsi, M.; Cristoforetti, G.; Palleschi, V.; Salvetti, A.; Tognoni, E. *Eur. Phys. J. D* **2001**, *13*, 373–377.

(25) Baldwin, J. M. *Appl. Spectrosc.* **1970**, *24*, 429–435.

(26) Stoian, R.; Rosenfeld, A.; Ashkenasi, D.; Hertel, I. V.; Bulgakova, N. M.; Campbell, E. E. B. *Phys. Rev. Lett.* **2002**, *88*, 097603.

(27) Anisimov, S. I. *Sov. Phys. JETP* **1968**, *27*, 182–183.

(28) Zel'dovich Y. B.; Raizer Y. P. *Physics of shock waves and high temperature hydrodynamics Phenomena*; Academic Press: New York, 1967.

(29) Mazhukin, V. I.; Nossov, V. V.; Nickiforov, M. G.; Smurov, I. *J. Appl. Phys.* **2003**, *93*, 56–66.

(30) Amoruso, S. *Appl. Phys. A: Mater. Sci. Process.* **1999**, *69*, 323–332.

(31) Liu, H. C.; Mao, X. L.; Yoo, J. H.; Russo, R. E. *Spectrochim. Acta, Part B* **1999**, *54*, 1607–1624.

(32) Amoruso, S.; Bruzzese, R.; Wang, X.; Xia, J. *Appl. Phys. Lett.* **2008**, *92*, 041503.

(33) Cheng, R.; Xu, X. F. *Phys. Rev. B* **2005**, *72*, 165415.

(34) Furusawa, K.; Takahashi, K.; Kumagai, H.; Midorikawa, K.; Obara, M. *Appl. Phys. A: Mater. Sci. Process.* **1999**, *69* (suppl.), S359–S366.

(35) Kittel C. *Introduction to solid state physics*; Wiley: New York, 1966.

(36) Margetic, V.; Bolshov, M.; Stockhaus, A.; Niemax, K.; Hergenröder, R. *J. Anal. At. Spectrom.* **2001**, *16*, 616–621.

(37) Fantoni, R.; Caneve, L.; Colao, F.; Fornarini, L.; Lazic, V.; Spizzichino, V. *Spectrochim. Acta, Part B* **2008**, *63*, 1097–1108.

(38) NIST electronic database; http://physics.nist.gov/PhysRefData; useful links on Atomic Spectroscopic Data on the Internet are at http://physics.nist.gov/PhysRefData/datarefs/IAU/WG1/chaptd.html.

(39) Castle, B. C.; Talabardon, K.; Smith, B. W.; Winefordner, J. D. *Appl. Spectrosc.* **1998**, *52*, 649–657.

(40) Griem, H. R. *Plasma Spectroscopy*; McGraw-Hill: New York, 1964.

(41) Konjevic, N.; Lesage, A.; Fuhr, J. R.; Wiese, W. L. *J. Phys. Chem. Ref. Data* **2002**, *31*, 819–927.

(42) Babina, E. M.; Il'in, G. G.; Konovalova, O. A.; Salakhov, M. Kh.; Sarandaev, E. V. *Publ. Astron. Obs. Belgrade* **2003**, *16*, 3–166.

(43) Robbiola, L.; Hurtel, L. P. Standard nature of the passive layers of buried archaeological bronze-the example of two Roman half- length portraits. In *Metal 95*; MacLeod, I., Pennec, S., Robbiola, L., Eds.; James and James Science Publ.: London, 1997; pp 109−117.

(44) Lazic, V.; Colao, F.; Fantoni, R.; Spizzichino, V. *Spectrochim. Acta, Part B* **2005**, *60*, 1002–1013.

(45) Gornushkin, S. I.; Gornushkin, I. B.; Anzano, J. M.; Smith, B. W.; Winefordner, J. D. *Appl. Spectrosc.* **2002**, *56*, 433–436.

(46) Irwin, A. W. *Astrophys. J., Suppl. Ser.* **1981**, *45*, 621–633.